Energy Engineering

Tech Science Press

https://doi.org/10.32604/ee.2026.076832

ARTICLE

Optimization Dispatch Strategy for Interconnected Shared Energy Storage Systems in Distribution Transformers Based on Regional Dynamic Partitioning

Ze'ang Ma[1], Jie Chen[2,*] and Shuai Lyu[3]

[1]School of Electrical Engineering, Shanghai Dianji University, Shanghai, China
[2]College of Electrical Engineering, Xinjiang University, Urumqi, China
[3]Extra-High Voltage Branch of State Grid Xinjiang Electric Power Co., Ltd., Urumqi, China

*Corresponding Author: Jie Chen. Email: xj_cj@163.com

Received: 27 November 2025; Accepted: 29 January 2026; Published: 12 November 2026

ABSTRACT: To address the operational volatility and complexity caused by the high penetration of renewable energy in distribution networks, the traditional static and isolated operation mode of distribution transformers struggles to simultaneously ensure power supply quality and economic efficiency. This paper proposes a coordinated dispatch strategy for interconnected distribution transformers based on regional dynamic partitioning and shared energy storage systems. Firstly, an improved K-means partitioning model for distribution transformers is constructed. By integrating a comprehensive distance metric that combines load characteristics and geospatial information, the limitations of traditional single-dimensional partitioning are overcome. Furthermore, a bi-level optimization dispatch model is established, with the upper-level objective of minimizing voltage deviation and the lower-level objective of minimizing operational cost, achieving the coordinated optimization of power quality and economic operation. On this basis, a comprehensive evaluation index composed of voltage stability and economic efficiency is innovatively proposed, and a dynamic weight adjustment mechanism feedback-based on the electrical correlation degree of distribution transformers is designed. This mechanism drives the closed-loop dynamic optimization of the partitioning scheme, enabling it to adaptively respond to the spatiotemporal changes of loads and renewable energy. Simulation results show that the proposed strategy increases the renewable energy utilization rate of distribution transformers by 5% and the daily maximum energy storage utilization rate by 9%, while forming a reasonable partitioning scheme with geographical compactness and electrical tightness.

KEYWORDS: Distribution transformer interconnection; renewable energy; shared energy storage; K-means; optimal operation

1 Introduction

With the acceleration of the global energy transition process, the penetration rate of renewable energy represented by photovoltaic (PV) systems in distribution networks has been continuously increasing [1]. However, the inherent intermittency and volatility of renewable energy have posed significant challenges to the safe and stable operation of distribution networks. The integration of high-penetration renewable energy not only causes problems such as voltage violations [2] and frequency fluctuations but also exacerbates the complexity of system operation [3]. The traditional static and islanded operation mode of distribution transformers struggles to achieve economic operation while ensuring power supply quality. Against this

Copyright © 2027 The Authors. Published by Tech Science Press. This work is licensed under a Creative Commons Attribution 4.0 International License, which permits unrestricted use, distribution, and reproduction in any medium, provided the original work is properly cited.

backdrop, improving system flexibility and economic efficiency through distribution transformer interconnection and coordinated dispatch has become an important research direction for the optimal operation of distribution networks.

Distribution transformer interconnection breaks the power supply isolation and realizes power mutual assistance; shared energy storage, acting as a "spatiotemporal energy regulator", effectively mitigates fluctuations and shifts loads. Existing studies have provided abundant insights for this context: To address the demand for simulating large-scale renewable energy grid integration and the insufficient optimization caused by improper parameter setting of heuristic algorithms, reference [4] proposes a distributed novel power system (DNPSs) model and a dynamic Levy flight-distributed multi-objective mantis search algorithm (DLFDMOMSA). The DNPSs can orchestrate the cooperative operation of six types of renewable energy sources, and the DLFDMOMSA avoids premature convergence of the algorithm through dynamic Levy flight parameter adjustment. Simulation results show that compared with seven comparison algorithms, the proposed algorithm can significantly reduce carbon dioxide emissions and generator costs in both 118- and 1375-bus novel power systems, and can obtain a better Pareto front curve with more advantageous optimization performance. Traditional distribution network scheduling mainly relies on system tools and empirical decision-making. However, with the large-scale integration of new energy sources, the complexity of power grid topology has brought significant security risks. To address this issue, reference [5] proposes a novel risk assessment method for distribution network scheduling operations. This method constructs probability models of wind power, photovoltaic power, and loads, and combines an improved Latin hypercube sampling technique to establish a quantitative assessment system with voltage over-limit and power flow overload as indicators. Simulation results demonstrate that the proposed method can effectively analyze the impact of new energy integration on scheduling risks, providing a theoretical basis for dispatchers to prevent and control risks in advance. To address the demand for intelligent scheduling in active distribution networks (ADNs), reference [6] proposes a multimodal artificial intelligence framework based on multi-agent reinforcement learning (MARL). This method innovatively fuses visual features of photovoltaic (PV) images with power grid electrical data, extracts PV soiling loss information via a CNN-ViT model, and adopts a decentralized MARL architecture to coordinately control multiple controllable resources. Experimental results demonstrate that the proposed method exhibits excellent performance in reducing operational costs, network losses, and carbon emissions, while significantly improving the flexibility and economic efficiency of power grid scheduling.

Addressing the problems of regional power–source and load imbalance as well as voltage fluctuations caused by the high–penetration integration of distributed generation, reference [7] constructs a three–layer coordinated planning model for a flexible interconnection system integrated with 5G base stations and their Backup Energy Storage Systems (BESS). By optimizing the system voltage and operating costs through hybrid algorithms, the reliability of power supply is improved. Targeting the AC–DC hybrid distribution network with multi–transformer area interconnection, reference [8] puts forward a two–layer coordinated optimal power scheduling method. Through the iterative optimization of the upper and lower layer models, remarkable results are achieved in reducing network loss and mitigating voltage fluctuations, which provides ideas for the structural optimization in constructing the "electrical–geographical" dual–dimension partitioning model in this paper. References [9] further advance the application of shared energy storage from the perspectives of system integration and business models. Reference [10] verifies the positive effect of shared energy storage in reducing system operating costs by constructing a coordinated operation framework between the Regional Integrated Energy System (RIES) and Distributed Energy Storage Aggregation Providers (DESAP). Furthermore, reference [11] establishes a bilevel optimization configuration model for shared energy storage in a Multi–Microgrid (MMG). It reveals the matching relationship between

energy storage parameters and renewable energy accommodation targets, which provides theoretical support for the design of dynamic evaluation indicators targeting economic efficiency and voltage stability in this paper. Collectively, these achievements indicate that structural optimization and business model innovation are the key paths to improving the comprehensive efficiency of the shared energy storage system, and also lay a solid foundation for the closed–loop optimization mechanism proposed in this paper.

Most existing studies conduct optimal dispatch based on fixed distribution transformer partitioning [12], lacking the dynamic adjustment capability for the coordinated optimization of partitioning structures and operational strategies. In addition, traditional partitioning methods for distribution transformers mostly rely on single-dimensional indicators (e.g., pure geographical distance), making it difficult to accurately reflect the electrical and geographical coupling relationships in actual systems. This results in deficiencies in the partitioning results regarding electrical tightness or geographical rationality. Therefore, there is a need for a distribution transformer partitioning and dispatch strategy that can integrate multi-dimensional information and possess dynamic response capabilities.

To address the aforementioned issues, this paper proposes a coordinated dispatch method for interconnected distribution transformers based on regional dynamic partitioning. Regional partitioning relies on switching devices. Compared with traditional mechanical switches, the Soft Open Point (SOP) possesses continuously controllable active and reactive power regulation capabilities, operates without restrictions on the number of operations, and features low power loss, thereby providing technical support for achieving flexible and reliable distribution transformer interconnection [13,14]. Structurally, this paper first constructs a comprehensive distance metric model integrating load characteristics and geospatial information, improving the traditional K-means clustering algorithm [15] to realize the electrical-geographical dual-dimensional optimization of distribution transformer partitioning. Furthermore, a bi-level optimization model with voltage stability and economic operation cost as the upper and lower objectives is established, and a comprehensive evaluation index and dynamic weight adjustment mechanism are designed to form a closed-loop optimization framework of "partitioning—dispatch—evaluation—adjustment". This strategy aims to achieve the coordinated dynamic optimization of distribution transformer partitioning and operational strategies, providing a new approach for the intelligent dispatch of distribution networks with high-penetration renewable energy integration.

2 Distribution Transformer Dispatch Model

2.1 Distribution Transformer Partitioning Model

The core of the basic K-means algorithm is to realize data clustering by optimizing an objective function, which aims to minimize the dispersion degree of data within clusters and make samples in the same cluster as similar as possible. This algorithm is widely applied in power grid optimization [16–18]. Assuming that the dataset $X = \{x_1, x_2, ..., x_n\}$ is partitioned into K clusters, and the center (centroid) of each cluster is $\mu_1, \mu_2, \ldots, \mu_k$, the objective function is defined as:

$$J = min \sum_{i=1}^{K} \sum_{x_i \in C_k} d_c \tag{1}$$

$$\mu_i^{new} = \frac{1}{|C_i|} \sum_{x_j \in C_i} x_j \tag{2}$$

The core idea of K-means is to minimize the objective function J and continuously update the centroids within clusters, so that the samples in each cluster are as evenly concentrated near the cluster center as possible, thereby achieving the clustering effect of "high intra-cluster similarity and low inter-cluster

similarity". K is the preset number of feeders; C_k is the K-th feeder cluster, containing feature vectors x_i; μ_i is the feature mean vector of the i-th feeder cluster. In feeder division, both the load characteristic distance and the geospatial distance need to be considered, and a comprehensive distance d_c is defined to replace the traditional Euclidean distance.

$$d_c = \sqrt{(1-\alpha)^2 \cdot d_{\text{load}}^2(x_{i,m}, \mu_i) + \alpha^2 \cdot d_{\text{geo}}^2(x_{i,m}, \mu_i)} \tag{3}$$

$$d_{\text{load}}(x_{i,m}, \mu_i) = \sqrt{\sum_{f=1}^{n} \left(\frac{x_{i,m,f} - \mu_{i,m,f}}{s_{i,m,f}} \right)^2} \tag{4}$$

$$s_{\text{i,m},f} = \sqrt{\frac{1}{N_K} \sum_{x_i \in C_k} \left(x_{i,m,f} - \overline{x} \right)^2} \tag{5}$$

$$d_{\text{geo}}(x_{i,m}, \mu_i) = \sqrt{(x_{i,m}^{\text{lat}} - \mu_i^{\text{lat}})^2 + (x_{i,m}^{\text{lon}} - \mu_i^{\text{lon}})^2} \tag{6}$$

α: Geographic distance weight ($0 < \alpha < 1$), usually taken as 0.4–0.6, controlling the priority of geographic compactness; $d_{\text{load}}(x_{i,m}, \mu_i)$: Characteristic distance between the load of station area i and the centroid load of station area i, where $x_{i,m}$ is the m-th load characteristic vector of station area i, containing n characteristic values; s_m is the standard deviation of this characteristic; μ_i is the centroid of station area i. $d_{\text{geo}}(x_{i,m}, \mu_i)$: Geographic coordinate distance between the m-th load of station area i and the centroid load of station area i, which is the Euclidean distance simplified by longitude and latitude calculation. This model reconstructs the "distance measurement rule" by weighting and fusing the simple load characteristic distance with the geographic spatial distance. When dividing station areas, it takes into account both the similarity of load characteristics and the proximity of geographic space, so as to avoid excessive span of station areas and unreasonable power supply radius. When iteratively updating the cluster centroid and reallocating samples, this comprehensive distance will be used to replace the traditional Euclidean distance, so that samples will be preferentially attributed to clusters with smaller comprehensive distances, making the divided station areas not only ensure similar load characteristics but also meet the requirement of geographic spatial compactness. The system diagram is shown in Fig. 1.

Constraints of the division model:

Constraint on the maximum input power of the station area

$$p_i \leq p_{max} \tag{7}$$

Constraint on the power supply radius of the station area

$$d_{\text{geo}} \leq R_{max} \tag{8}$$

$$d_{\text{geo}}(\text{m}_1) - d_{\text{geo}}(\text{m}_2) \leq R_{set} \tag{9}$$

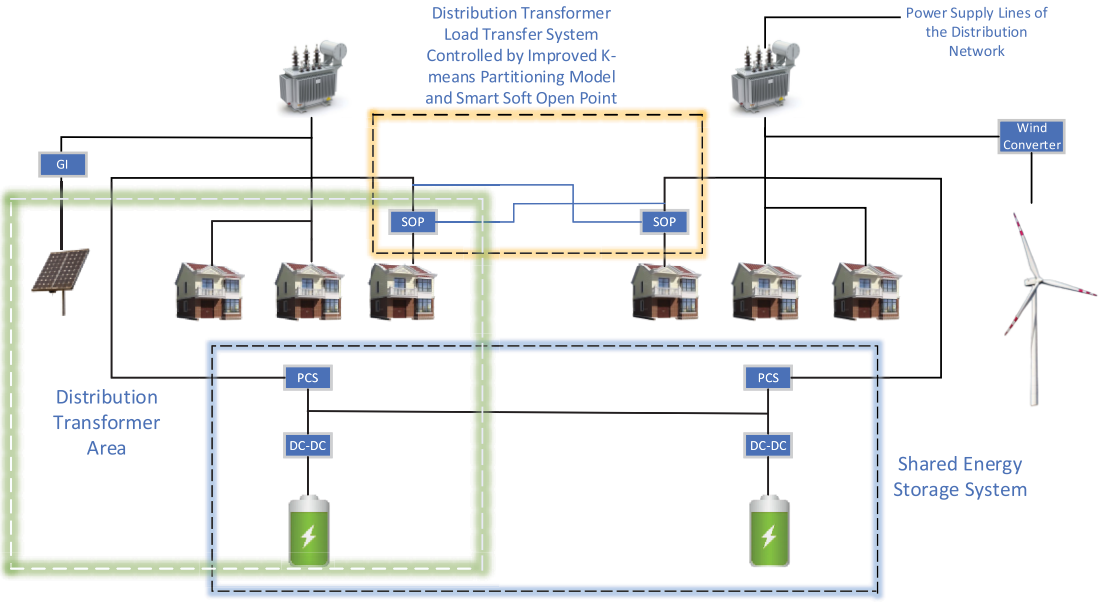


Figure 1: Diagram of the station area interconnection system.

2.2 Upper-Layer Function

$$minV_{\text{syn}} = \beta_1 V_{\text{ben}} + \beta_2 V_{\text{mom}} + \beta_3 V_{\text{vol}} \tag{10}$$

$$V_{\text{ben}} = \frac{1}{\text{k}} \frac{1}{T} \sum_{i=1}^{\text{k}} \sum_{t=1}^{T} \left| \frac{V_{i,t} - V_{\text{N}}}{V_{\text{N}}} \right| \tag{11}$$

$$V_{\text{mom}} = \frac{1}{\text{k}} \frac{1}{T-1} \sum_{i=1}^{\text{k}} \sum_{t=1}^{T-1} \left| \frac{V_{i,t+1} - V_{i,t}}{V_{i,t}} \right| \tag{12}$$

$$V_{\text{vol}} = \max \left\{ \left| \frac{V_{i,max} - V_{\text{N}}}{V_{\text{N}}} \right|, \left| \frac{V_{i,min} - V_{\text{N}}}{V_{\text{N}}} \right| \right\} \tag{13}$$

This distribution station area voltage regulation model comprehensively considers three indicators: voltage benchmark deviation V_{ben}, voltage moment deviation V_{mom}, and maximum voltage deviation V_{vol}, and introduces weights. Compared with the single–indicator model, this model can more comprehensively reflect the voltage deviation level. The goal of the upper–layer planning is to minimize the weighted value of the above three indicators. In the formula, β is the weight value, determined based on empirical values. $V_{i,t}$ is the main line voltage of station area k at time t, and $V_{i,min}$, $V_{i,max}$ are the minimum and maximum values of the main line voltage of station area k.

Constraint conditions

$$V_{i,t} = V_0 - \sum_{j \in \mathcal{N}_i} R_{ij} \cdot \left(\frac{P_{\text{net}}^j(t)}{V_N} \right) \tag{14}$$

$$P_{\text{net}}^j(t) = P_{\text{load}}^j(t) - P_{pv}^j(t) - P_{pw}^j(t) - P_{\text{bat}}^j(t) - \sum_m P_{L,t}^{jm} \tag{15}$$

$$V_{\text{min}} \le V_{i,t} \le V_{\text{max}} \tag{16}$$

$P^j_{load}(t)$ is the load power of node j at time t (a positive value indicates power consumption); $P^j_{pv}(t)$ is the photovoltaic power generation power of node j at time t; $P^j_{pw}(t)$ is the wind power generation of node j at time t; $P^j_{bat}(t)$ is the charging and discharging power of the energy storage at node j at time t. A positive value indicates discharging (injecting power into the power grid), and a negative value indicates charging (absorbing power from the power grid); $\sum_m P^{jm}_{L,t}$ is the total power transmitted by node j to other nodes (denoted by m) through tie lines. When node j transmits power to node m, $P^{jm}_{L,t}$ is positive; when node m transmits power to node j, it is recorded as a negative value. In fact, the tie–line power is bidirectional, so this term already includes all tie–line powers (inflow and outflow) connected to node j. This paper employs a linearized voltage calculation formula based on the simplified DistFlow power flow model for voltage fluctuation assessment. This model linearizes the power-voltage relationship of distribution network branches, expressing the node voltage magnitude as the sum of the reference point voltage and the voltage drops caused by the active power flow in each branch. This method offers good computational efficiency and practicality in radial distribution networks, making it particularly suitable for rapid voltage assessment in feeder-level scheduling optimization. In scenarios with high penetration of renewable energy and power support between feeders, significant reactive power flow and voltage phase angle changes may occur, which the linear model might not fully capture due to the coupling effect between voltage magnitude and phase angle. To evaluate the impact of model simplification on scheduling results, selected scenarios are simulated to compare the voltage calculation results of the simplified DistFlow model and the AC power flow model. The results indicate that in the interconnected feeder system studied, node voltage deviations remain within ±5% in the vast majority of cases, meeting the accuracy requirements for engineering dispatch. Future work may introduce second-order cone relaxation or neural network-based voltage prediction models to enhance voltage modeling accuracy in high-penetration scenarios.

2.3 Lower–Layer Objective Function

The core objective is to reduce the overall operating cost of energy storage power stations to the greatest extent, so as to maximize economic benefits.

$$\min C_{\text{opera}} = \gamma_1 c_{\text{buy}} + \gamma_2 c_{\text{loss}} + \gamma_3 c_{\text{life}} \tag{17}$$

$$c_{\text{buy}} = \sum_{i=1}^{k} \sum_{t=1}^{T} P^i_{\text{buy}}(t) \text{w}_{\text{buy}}(t) \tag{18}$$

$$C_{\text{loss}} = \left(P_{\text{pcs,loss}} + P_{\text{dc,loss}} + P_{\text{bat,loss}} + P_{\text{L,loss}}\right) \Delta t \cdot \overline{\omega}_{\text{line}} \tag{19}$$

$$C_{\text{life}} = C_{\text{bat}} + C_{\text{trans}} \tag{20}$$

The overall operating cost C_{opera} of the energy storage power station includes the electricity purchase cost from the external power grid c_{buy} (equal to the product of the power $p^i_{\text{buy}}(t)$ output by the power grid system of the i-th station area at time t and the electricity price $w_{\text{buy}}(t)$ at time t), the power loss cost C_{loss} during the operation of the shared energy storage system (including the power loss costs of the shared energy storage power station, energy storage converter PCS, DC–DC, and DC tie lines), and the life loss cost C_{life} (including the battery life loss cost of the energy storage system and the transformer life loss cost). $\overline{\omega}_{\text{line}}$ is the average electricity price, and γ_1, γ_2, γ_3 are weight coefficients. These weights correspond to the relative importance of power purchase cost, loss cost, and lifespan degradation cost within the total operational cost. The determination of these weights is based on the Analytic Hierarchy Process (AHP), integrating expert ratings with actual system operational data, and is calculated through pairwise comparison matrices.

$$P_{\mathrm{pcs,loss}} = \sum_{i=1}^{k}\sum_{t=1}^{\mathrm{T}} \eta_{\mathrm{pcs}} \left|P_{\mathrm{pcs}}^{i}(t)\right| \tag{21}$$

$$P_{\mathrm{dc,loss}} = \sum_{i=1}^{k}\sum_{t=1}^{T} \eta_{\mathrm{dc}} \left|P_{\mathrm{dc}}^{i}(t)\right| \tag{22}$$

$$P_{\mathrm{bat,loss}} = \sum_{i=1}^{k}\sum_{t=1}^{T} (1-\eta_{\mathrm{bat}}) \left|P_{\mathrm{bat}}^{i}(t)\right| \tag{23}$$

$$P_{L,loss} = \sum_{1\le i<j\le k} \left(\sum_{t=1}^{T} \left(\frac{P_{\mathrm{Ls},t}^{\mathrm{ij}}}{U_{\mathrm{dc}}} \right)^{2} R_{\mathrm{ij}} \right) \tag{24}$$

In the formula: $P_{\mathrm{pcs,loss}}$ is the power corresponding to the PCS loss; $P_{\mathrm{pcs}}^{i}(t)$ is the power flowing through the PCS of the i-th distribution transformer area at time t; η_{pcs} is the loss coefficient of PCS; $P_{\mathrm{dc}}^{i}(t)$ is the power flowing through the DC-DC of the i-th distribution transformer area at time t; $P_{\mathrm{dc,loss}}$ is the power corresponding to the DC-DC loss; η_{dc} is the loss coefficient of DC-DC; $P_{\mathrm{bat,loss}}$ is the power loss of the battery; $P_{\mathrm{bat}}^{i}(t)$ is the battery power of the i-th distribution transformer area at time t; a negative value of $P_{\mathrm{bat}}^{i}(t)$ indicates charging, and a positive value indicates discharging; η_{bat} is the charge-discharge efficiency of the battery; $P_{L,loss}$ is the power loss on the DC interconnection line between each transformer area; U_{dc} is the DC-side voltage level; $P_{\mathrm{Ls},t}^{\mathrm{ij}}$ is the power loss on the DC interconnection line between transformer area i and transformer area j at time t; R_{ij} is the resistance of the DC interconnection line between transformer area i and transformer area j.

2.4 Battery Life Loss Cost

The charge–discharge depth of a battery is closely related to its lifespan. Generally speaking, the deeper the battery discharge depth, the shorter the operating lifespan. Based on the research foundation of references [19–21], the lithium–ion battery cycle life loss cost function is derived as

$$c_{\mathrm{bat}} = \sum_{i=1}^{\mathrm{k}}\sum_{t=1}^{T} \frac{C_{\mathrm{inv}}^{i}\left|P_{\mathrm{bat}}^{i}(t)\right|}{N_{\mathrm{life}} \times 365 \times 24 \times Q_{\mathrm{N}}^{i}} \Delta t \tag{25}$$

$$C_{\mathrm{inv}}^{i} = c_{\mathrm{p}} P_{\mathrm{N}}^{i} + c_{\mathrm{Q}} Q_{\mathrm{N}}^{i} \tag{26}$$

In the formula: C_{inv}^{i} is the initial investment cost of shared energy storage in area i; N_{life} is the service life of shared energy storage; Q_{N}^{i} is the capacity of the battery in area i; P_{N}^{i} is the rated power; c_{p} and c_{Q} are the unit capacity investment cost and unit power investment cost of the battery, respectively.

2.5 Transformer Life Loss Cost

The transformer cost is mainly related to material aging (expected service life) and operating load. Combined with references [22,23], its life loss cost function is derived as

$$C_{\mathrm{Ttrans}} = \sum_{i=1}^{K} \frac{C_{\mathrm{iov},i} \sum_{t=1}^{\mathrm{T}} \left|P_{\mathrm{load},i}(t)\right|}{N_{\mathrm{life},i} \times 365 \times 24 \times S_{N,i}} \Delta t \tag{27}$$

$C_{\mathrm{iov},i}$ is the initial investment cost of the transformer in area i; $P_{\mathrm{load,k}}(t)$ is the load power of area i at time t; $N_{\mathrm{life},k}$ is the design life of the transformer in area i; $S_{N,k}$ is the rated capacity of the transformer in area i.

Constraint conditions:

$$P_{buy}^{i}(t) = P_{load}^{i}(t) - P_{pv}^{i}(t) - P_{pw}^{j}(t) - P_{bat}^{i}(t) - \sum_{j}\left(P_{L,t}^{ij} - P_{L,t}^{ji}\right) \tag{28}$$

$$\left|P_{L,t}^{ij}\right| \le P_{L,max}^{ij} \tag{29}$$

2.6 Battery SOC Constraints

Overcharging and over-discharging of batteries are likely to trigger internal chemical reactions, degrade electrode materials, and thereby shorten the service life of the energy storage system. Therefore, it is necessary to control the state of charge (SOC) of the energy storage system within a reasonable range. To ensure the continuity of shared energy storage operation, it is a reasonable requirement to keep the SOC consistent at the start and end of the scheduling cycle, as shown in the following formula:

$$-P_{\mathrm{N}}^{i} \le P_{\mathrm{bat}}^{i} \le P_{\mathrm{N}}^{i} \tag{30}$$

$$SOC^{i}(1) = SOC^{i}(24) \tag{31}$$

$$SOC^{i}(t) = SOC^{i}(t_0) + \sum_{\tau=t_0}^{t} \frac{P_{\mathrm{bat}}^{i}(\tau)\Delta t}{Q_{\mathrm{N}}^{i}} \tag{32}$$

$$-P_{\mathrm{N}}^{i} \le P_{\mathrm{bat}}^{i} \le P_{\mathrm{N}}^{i} \tag{33}$$

In the formula: $SOC_{\max}^{i}$ and $SOC_{\min}^{i}$ are the upper and lower limits of the SOC of the battery in area i; SOC_{t}^{i} is the SOC of the battery in area i at time t; $SOC^{i}(1)$ is the SOC of area i at the initial moment of the set scheduling cycle; $P_{pv}^{i}(t)$ is the value of photovoltaic power generation in area i at time t.

2.7 Solution of the Bi-Level Optimization Model and Convergence Analysis

2.7.1 Solution Algorithm Design

The bi-level optimization model established in this paper aims at optimal voltage stability in the upper level and minimal operational cost in the lower level. Due to the coupling between the two levels (e.g., tie-line power, energy storage charge/discharge states), direct solution is complex. Therefore, this paper employs a bi-level iterative algorithm based on sensitivity analysis. The specific steps are as follows:

Step 1: Initialization. Set the initial feeder partition scheme (e.g., based on historical data or a fixed partition), initialize state variables such as energy storage SOC and tie-line power, and set the maximum number of iterations to 50.

Step 2: Lower-Level Optimization Solution. Solve the lower-level economic dispatch model under given upper-level decision variables. This model is a typical nonlinear programming problem. This paper employs an Improved Particle Swarm Optimization (IPSO) algorithm for solution, which is suitable for optimization scenarios with multiple constraints and variables. An adaptive inertia weight adjustment mechanism is introduced in the algorithm to enhance the balance between global and local search capabilities.

Step 3: Upper-Level Optimization Solution. Based on the results of the lower-level optimization (e.g., power distribution and actual voltage values at each time step), calculate the current voltage stability index, V_{syn}. Then, optimize the upper-level voltage adjustment model using the Sequential Quadratic Programming (SQP) method to update the voltage reference values and tie-line power limits.

Step 4: Bi-Level Information Exchange and Iteration. Transfer the updated upper-level optimization results to the lower level to perform economic dispatch again. Subsequently, feed the re-optimized power distribution and voltage states from the lower level back to the upper level. This cycle iterates until the convergence criteria are met.

Convergence Criterion: The process is considered converged if the change in the objective function between two consecutive iterations is less than a predefined threshold, expressed as:

$$|V_{syn}^{(iter)} - V_{syn}^{(iter-1)}| < \varepsilon_1 \tag{34}$$

$$|C_{opera}^{(iter)} - C_{opera}^{(iter-1)}| < \varepsilon_2 \tag{35}$$

If this condition is satisfied, the algorithm is considered converged, and the optimal dispatch scheme is outputted.

2.7.2 Convergence Analysis

The proposed bi-level iterative algorithm can be mathematically regarded as a cooperative descent process. Its convergence can be analyzed from the following two aspects: Monotonicity and Boundedness of the Objective Functions: Both the upper-level objective V_{syn} and the lower-level objective C_{opera} have clear physical meanings and mathematical lower bounds (e.g., non-negative voltage deviation, non-negative cost). In each iteration, the lower-level optimization seeks cost minimization with fixed upper-level variables, while the upper-level optimization pursues optimal voltage stability based on fixed lower-level results. Both constitute convex (or approximately convex) optimization problems, ensuring that the objective function value decreases or remains unchanged in every iteration.

Stability of the Iterative Process: Oscillation or divergence during iterations is prevented by introducing step-size limits and variable boundary constraints (e.g., voltage limits, power limits). In the simulation experiments, with $\varepsilon_1 = 10^{-4}$ and $\varepsilon_2 = 10^{-3}$ set, the algorithm typically converges within 10–15 iterations. The resulting convergence curve is smooth and stable, indicating favorable numerical stability of the algorithm.

To verify the convergence and stability of the proposed bi-level iterative algorithm, this subsection monitors the optimization process under a typical scenario (with K = 3 and $\alpha = 0.5$). The values of the upper-level voltage stability objective V_{syn} and the lower-level operational cost C_{opera} are recorded for each iteration. The results are shown in Fig. 2.

This closed-loop optimization process can be mathematically formulated as an iterative optimization problem, with the comprehensive evaluation metric Q_k serving as its objective function. The method is expected to converge to a local optimum within a finite number of iterations, based on the following reasoning: (1) Q_k is composed of voltage stability and operational cost terms, both of which are convex or quasi-convex functions within a reasonable operating range; (2) The adjustment strategies for parameters K and α are based on heuristic search, with each iteration designed to reduce Q_k; (3) In simulations, Q_k consistently decreases and eventually stabilizes as the number of iterations increases.

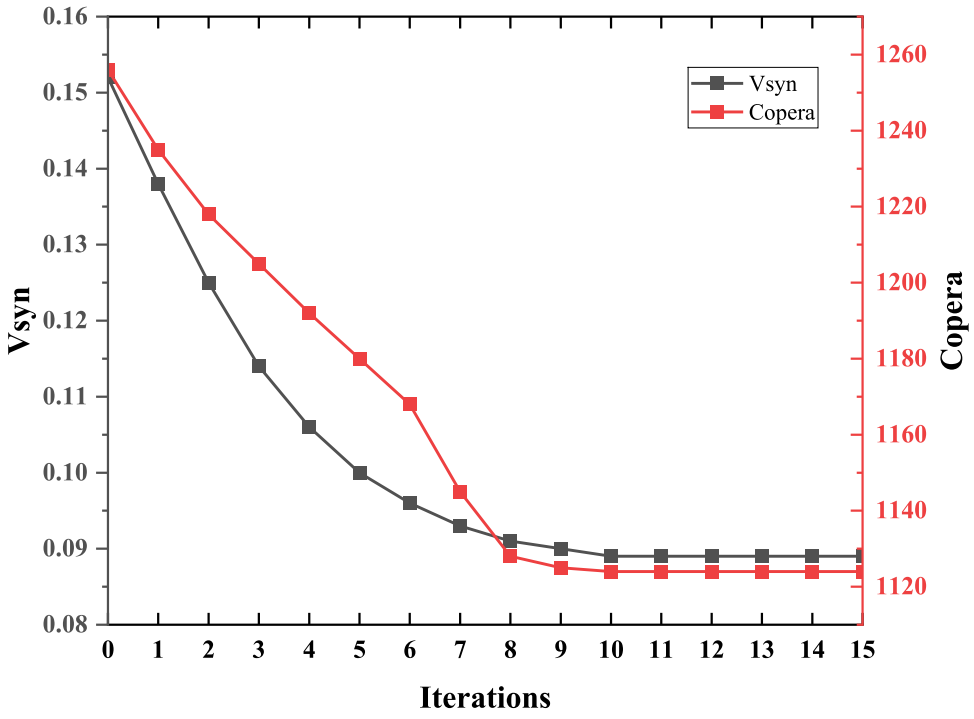


Figure 2: Convergence curve of the bi-level optimization algorithm.

3 Dynamic Division

3.1 Define the Comprehensive Evaluation Index Q_k for Division

$$Q_k = \beta \cdot \frac{V_{syn}}{V_{syn0}} + \gamma \cdot \frac{C_{opera}}{C_{opera0}} \tag{36}$$

$$\beta + \gamma = 3 \tag{37}$$

V_{syn0} and C_{opera0} are reference values, which are the values when all transformer areas operate independently without interconnection scheduling, and are used for normalization to eliminate the influence of dimension. β and γ are empirical coefficients, reflecting the degree of emphasis on voltage stability and economy. The calculation goal is to find the transformer area division scheme that minimizes the comprehensive evaluation index Q_k.

3.2 Finding the Optimal Number of Transformer Areas K

Set the search range: Based on the scale of the distribution network, define a range for the number of station areas $2 \leq K \leq 10$. For each candidate value of k, the process is as follows: First, partitioning: use the adjusted *k*-means algorithm to divide all nodes into *k* clusters. Second, scheduling: based on this partitioning scheme, execute the upper-layer voltage adjustment model and the lower-layer economic dispatch model. Third, evaluation: calculate the comprehensive evaluation indicator Q_k under this partitioning scheme. Finally, decision-making: compare all Q_k values and select the k value that minimizes Q_k as the optimal number of station areas Q_{best}.

3.3 Dynamically Adjusting Distance Weight α

For any two districts i and j, calculate their average power exchange intensity within a scheduling cycle: Define the electrical correlation degree E_{ij} of the districts.

$$E_{ij} = \frac{1}{T}\sum_{t=1}^{\mathrm{T}} |P_{L,t}^{ij}| \tag{38}$$

This is a very important indicator, representing the exchange power of each district within a cycle. $P_{L,t}^{ij}$ is the power on the DC tie line between district i and district j at time t. The larger E_{ij} is, the closer the electrical connection between the two districts is. It indicates that the loads of the two districts differ greatly, suggesting that the current α value (geographical weight) may be too high, causing the algorithm to place too much emphasis on geographical distance while ignoring electrical connections. This model will reduce the α value, decrease the weight of geographical distance, and increase the weight of load characteristic distance. If it is found that the electrical correlation degree of a district is relatively low, α can be appropriately increased to raise the weight of geographical distance and make the geographical distribution more compact. $E_{\max}$ and $E_{\min}$ are the set maximum and minimum values. Set the upper and lower limits of α as $\alpha \in [0.2, 0.8]$ to prevent excessive adjustment. μ is the attenuation factor, with a set value of 0.1.

$$f\left(\alpha^{(t)}\right) = \begin{cases} \min(0.8, \alpha_{old} \cdot (1+\mu)) & if\ E_{ij} > E_{\max} \\ \max(0.2, \alpha_{old} \cdot (1-\mu)) & else\ if\ E_{ij} < E_{\min} \\ \alpha_{old} & otherwise \end{cases} \tag{39}$$

$$\alpha^{(t+1)} = f\left(\alpha^{(t)}\right) \tag{40}$$

After adjustment, α is used to re-perform the clustering division for the current k value and the calculation of the electrical correlation degree of districts. When the judgment condition is satisfied or the cyclic calculation reaches the specified number of times, the optimized α_{new} is output.

3.4 Application and Iteration

The obtained optimal parameters K_{best} and α_{new} are used for the district division in the next operation cycle. This process can be repeated every cycle (or every several cycles), so that the district division can dynamically adapt to changes in conditions such as load and photovoltaic. The operational flow chart is illustrated in Fig. 3. Some parameters involved in the simulation experiment are as follows: η_{pcs} = 5%, η_{dc} = 1%, η_{bat} = 93.5%, U_{dc} = 750 V, $\overline{\omega}_{\mathrm{line}}$ = 1.3 yuan/kW·h, c_{p} = 320 yuan/kW·h, c_{Q} = 1000 yuan/kW·h, $C_{\mathrm{iov,i}}$ = 500 yuan/kW · h, P_{N} = 50 kW, Q_{N} = 62.7 kW·h, $SOC_{\min}$ = 0.1, $SOC_{\max}$ = 0.9.

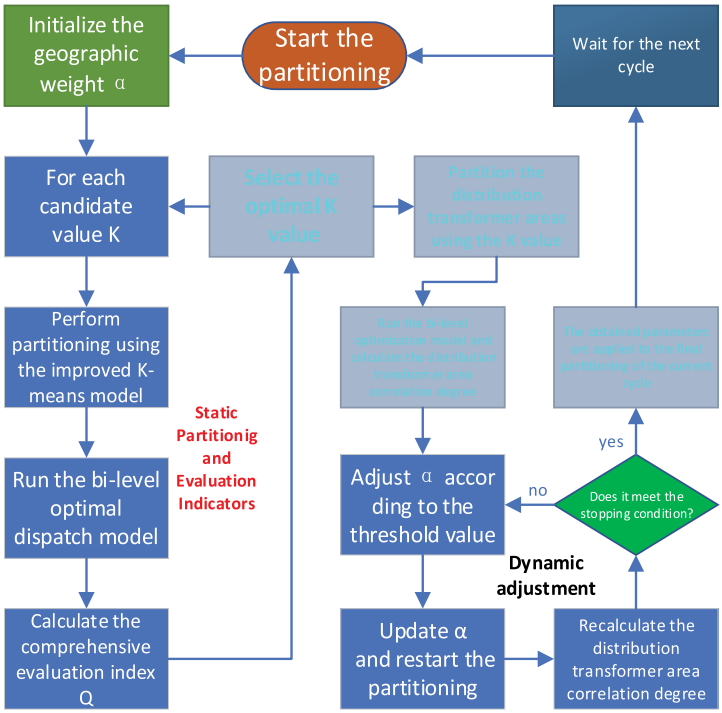


Figure 3: The operational flow chart.

3.5 Sensitivity Analysis and Parameter Justification

To ensure the robustness of the proposed dynamic partitioning mechanism, a sensitivity analysis is conducted on the geographical weight α and its adjustment step size μ, aiming to verify their impact on clustering stability and system economy.

3.5.1 Determination of the Parameter α Range

The geographical weight α balances the roles of load characteristic similarity and geographical proximity in the clustering process. To determine its reasonable bounds, the following experiment is designed: while keeping other parameters fixed $K = 3$, $\mu = 0.1$, α is increased from 0.1 to 1.5 in increments of 0.1. For each value of α, the clustering quality index (silhouette coefficient) and the system comprehensive performance index Q are calculated. The experimental results indicate that: when $\alpha < 0.2$, geographical distance is almost ignored, leading to excessively dispersed feeder spatial distribution, an overly large power supply radius, and a relatively low silhouette coefficient. This outcome fails to meet the practical engineering constraints of distribution networks. When $\alpha > 0.8$, the load characteristic information is excessively weakened, resulting in reduced power complementarity within feeders and a higher system comprehensive performance index. When α lies within the interval [0.2, 0.8], the system comprehensive performance remains relatively stable, with minimal fluctuation in the Q value. As shown in Fig. 4, α is ultimately constrained to [0.2, 0.8]. This range ensures reasonable partitioning while providing sufficient flexibility for dynamic adjustment.

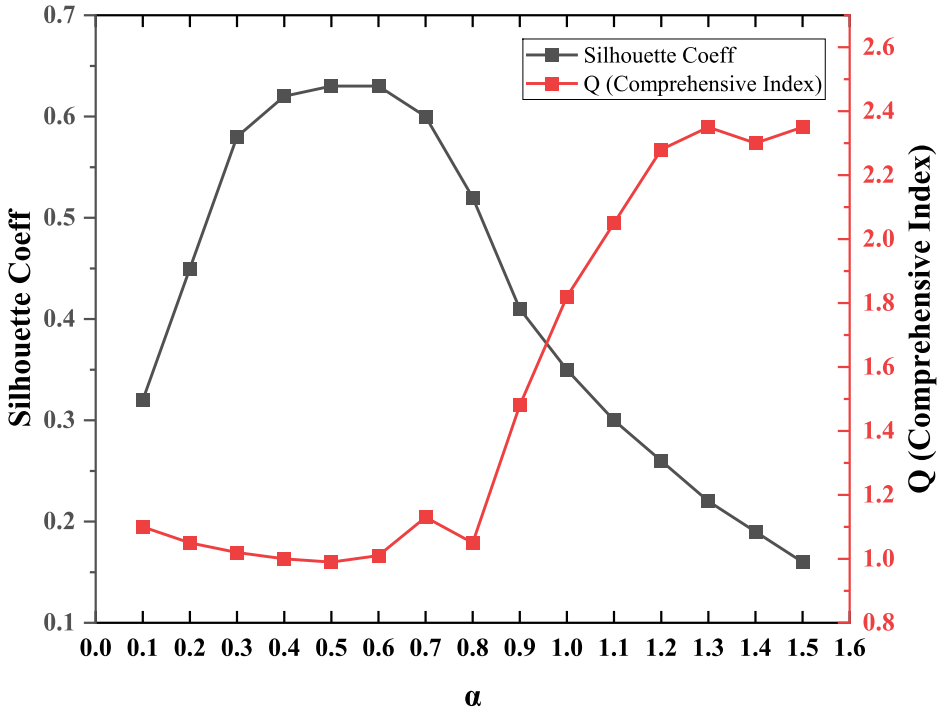


Figure 4: Effect of the geographical weight α on clustering quality and system performance.

3.5.2 Determination of the Attenuation Factor μ

The attenuation factor μ controls the magnitude of the dynamic adjustment for α, influencing the algorithm's convergence speed and stability. Through multi-period simulations comparing the adjustment effects under μ = 0.05, 0.1, 0.15, and 0.2, it is found that: An excessively small μ (e.g., 0.05) leads to slow adjustment, making it difficult to adapt to rapid changes in load and renewable energy; an excessively large μ (e.g., 0.2) tends to cause oscillations in the α value, adversely affecting partitioning stability. With μ = 0.1, the algorithm achieves a sound balance between convergence speed and stability, typically enabling smooth adjustment of α within 3–5 cycles. Fig. 5 illustrates the influence of α and μ on the comprehensive index Q. It can be observed that the system performance is most stable when $\alpha \in [0.2, 0.8]$ and μ = 0.1, which validates the rationality of the parameter settings.

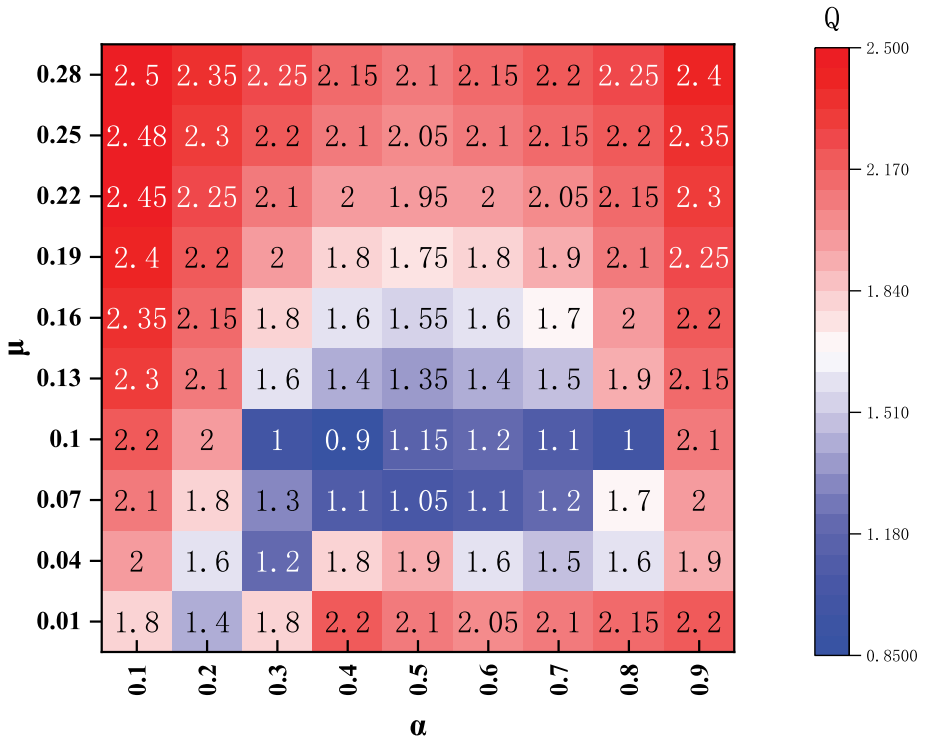


Figure 5: Heatmap analysis of the effects of geographical weight α and attenuation factor μ on the comprehensive performance index Q.

3.6 Stability Discussion

Under fluctuations of renewable energy and load, whether the partitioning results will oscillate depends on the following factors: (1) The smoothness of the calculated electrical correlation degree E_{ij}. In this study, moving average processing is applied to the electrical correlation degree to smooth out fluctuations. (2) The reasonableness of the weight adjustment mechanism, including appropriate step sizes and upper/lower limits. The parameter settings in this paper (e.g., $\alpha \in [0.2, 0.8]$, $\mu = 0.1$) have been validated through sensitivity analysis. (3) The adaptability of the partition update frequency to the rate of system changes. Partitions are updated at each dispatch cycle (or every several cycles) rather than in real-time. Simulation results demonstrate the stable variation of K and α across multiple cycles, indicating that the system can maintain the stability of the partitioning scheme even under typical fluctuation scenarios.

4 Simulation Data

The simulation software used in this paper is MATLAB 2020b, which includes updates for multiple toolboxes. For example, the Deep Learning Toolbox has added support for importing TensorFlow 2 and PyTorch models, strengthening the deep learning workflow. The Signal Processing Toolbox has enhanced its spectrum analysis and filter design functions. This version has also optimized the interactive experience of the Live Editor, improved integration capabilities with other programming languages, and enhanced performance for calculations involving large datasets and complex models. It provides more efficient tool support for fields such as engineering calculations, data analysis, and algorithm development.

Taking the first cycle as an example, to verify the effectiveness of the interconnected district scheduling strategy based on regional dynamic division proposed in this paper, we conduct simulation analysis on the system performance under different district numbers (K = 1~10) to select the optimal K value and α value.

The results are shown in Fig. 6. The figure displays the curves of the comprehensive evaluation index Q value, voltage stability index, system operation cost, and geographical weight α value with the change of district number K from top to bottom in sequence. The simulation results show that for comprehensive performance (Q value), when the district number K = 3, the comprehensive evaluation index Q value reaches the lowest, indicating that the system achieves the best balance between voltage stability and economy at this time, which verifies the effectiveness of the dynamic division strategy proposed in this paper. If the K value is too small (such as K = 2) or too large (such as K > 5), the Q value will increase and the overall system performance will decline. For voltage stability, the voltage stability index reaches the optimal (the lowest value) when K = 3, indicating that reasonable district interconnection and division can effectively suppress voltage fluctuations and improve power quality. As the K value continues to increase, the voltage stability tends to be stable.

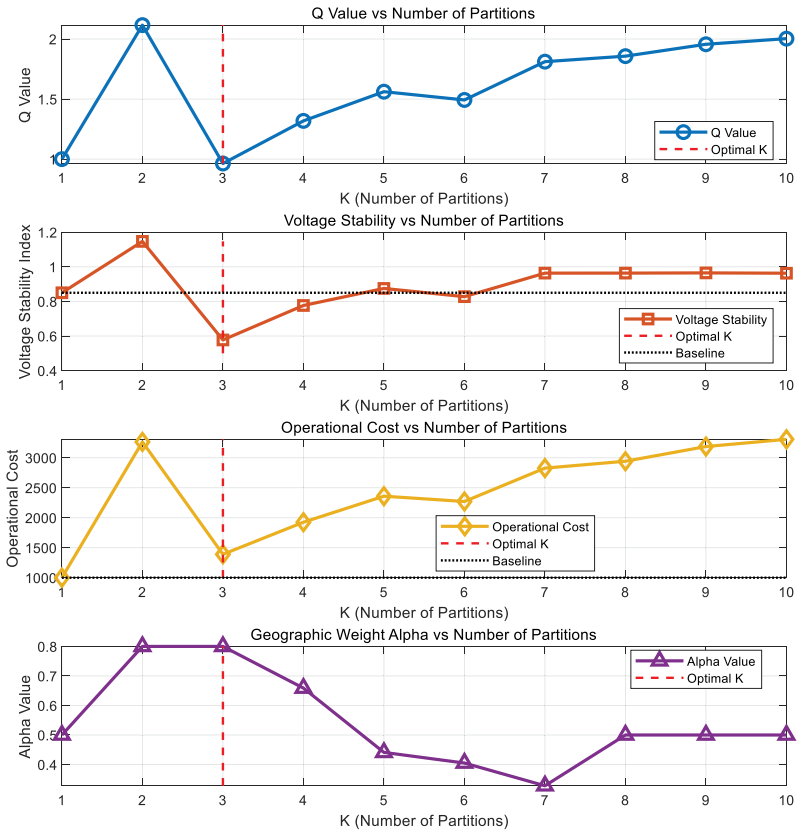


Figure 6: Curves of system comprehensive performance indicators under different district division numbers.

Economic operation cost: The system operation cost when K = 3 is slightly higher than that in the island operation mode K = 1. This is mainly due to the losses of tie lines and energy storage. When K > 4, the cost rises slowly. Adaptive adjustment of geographical weight: The geographical distance weight α is dynamically adjusted with the change of K value, and it is relatively high when K = 3. This indicates that the algorithm pays more attention to geographical spatial constraints in this environment, reflecting the adaptive effect of the algorithm in changing parameters according to the environment.

The most prominent feature in Fig. 7 is the appearance of three distinct yellow bright blocks along the diagonal, which are clearly separated by blue boundary lines. The color inside each yellow bright block is very bright, indicating that the electrical correlation between each node within the same district is extremely high. This achieves the goal of "high intra-cluster similarity" in the model, demonstrating that the electrical

connections within each divided district are very close. The areas outside the red blocks, especially the areas between the bright blocks, are dark blue, which indicates that the electrical correlation between nodes of different districts is low. This achieves the design goal of "low inter-cluster similarity", showing that the electrical independence between different districts is strong. The red solid lines in the figure clearly mark the boundary of each district. It can be seen that the algorithm successfully divides 50 nodes into 3 districts with close electrical connections.

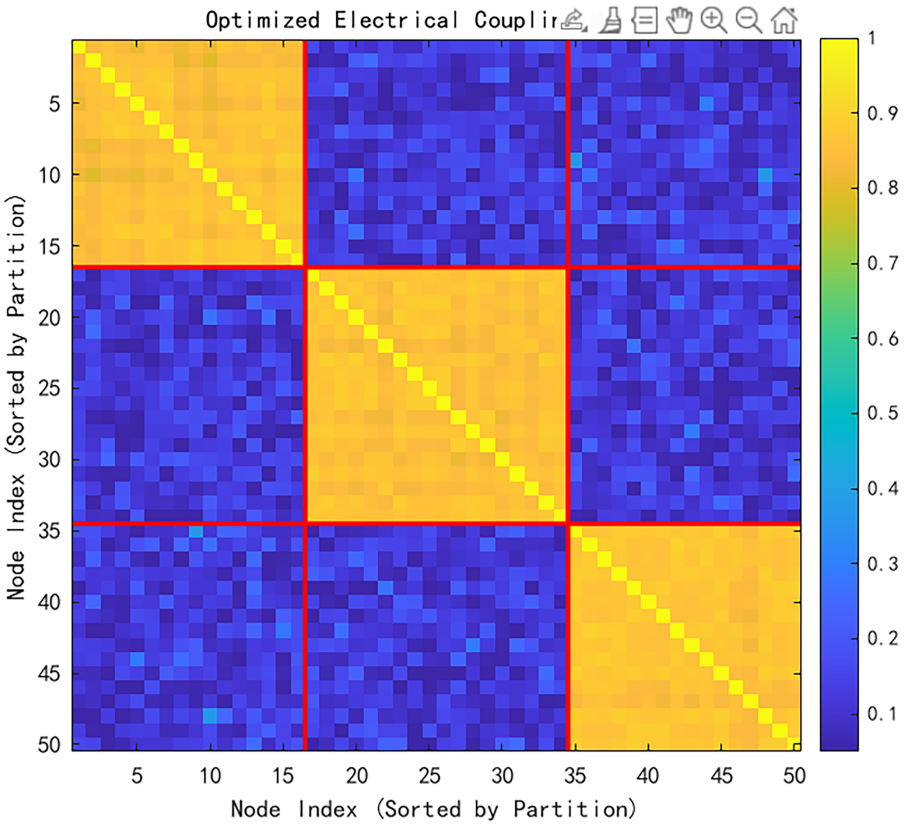


Figure 7: Optimized district electrical correlation matrix.

To verify the dynamic adaptability of the proposed algorithm, a multi-cycle simulation experiment was designed, simulating five typical operating scenarios: a typical working day, another working day, a weekend, a rainy day, and a high-temperature day. As shown in Fig. 8, the algorithm can perceive changes in load and new energy under different scenarios, and automatically adjust the optimal number of station areas K and geographical weight α, demonstrating excellent dynamic adaptability. Especially in weekend and high-temperature scenarios, the algorithm effectively responds to changes in load patterns by adjusting the partitioning strategy, maintaining the economic operation and voltage stability of the system.

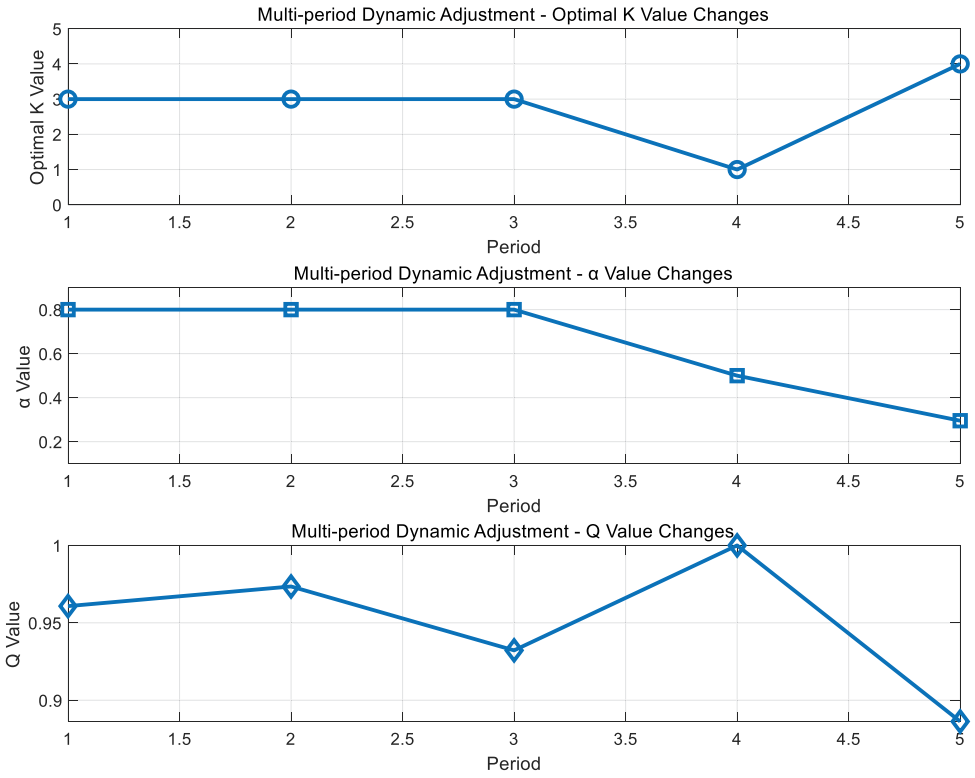


Figure 8: Multi-cycle system parameter variation diagram.

Figs. 9 and 10 present the generator output diagrams before and after optimization. It can be observed that after optimization, the proportion of load power supplied by renewable energy and energy storage systems has increased, and the interconnected system has also shared part of the load power. From Figs. 11 and 12, it can be intuitively seen that the utilization rates of energy storage and renewable energy in the improved system have both been enhanced. Compared with the traditional mode, the improved strategy, through dynamic partitioning and coordinated dispatch of distribution transformer areas, enables renewable energy output to more accurately match the load demand of each area, thereby reducing the curtailment of wind and photovoltaic power caused by output fluctuations or supply-demand mismatch. Meanwhile, the cross-district complementary dispatch capability of the shared energy storage system has been fully exploited. During off-peak periods, it centrally charges to store surplus renewable energy power, and during peak periods, it discharges directionally to support loads—this not only reduces the waste of renewable energy output but also improves the cyclic utilization efficiency of energy storage equipment. Data shows that compared with the traditional mode, the renewable energy utilization rate after improvement has increased by up to approximately 8%, and the daily energy storage equipment utilization rate has the maximum increase of 9%. This effectively addresses the industry pain point of "difficult absorption and low utilization" under high-proportion renewable energy integration, further verifying the advantages of the dynamic partitioning strategy in improving energy utilization efficiency.

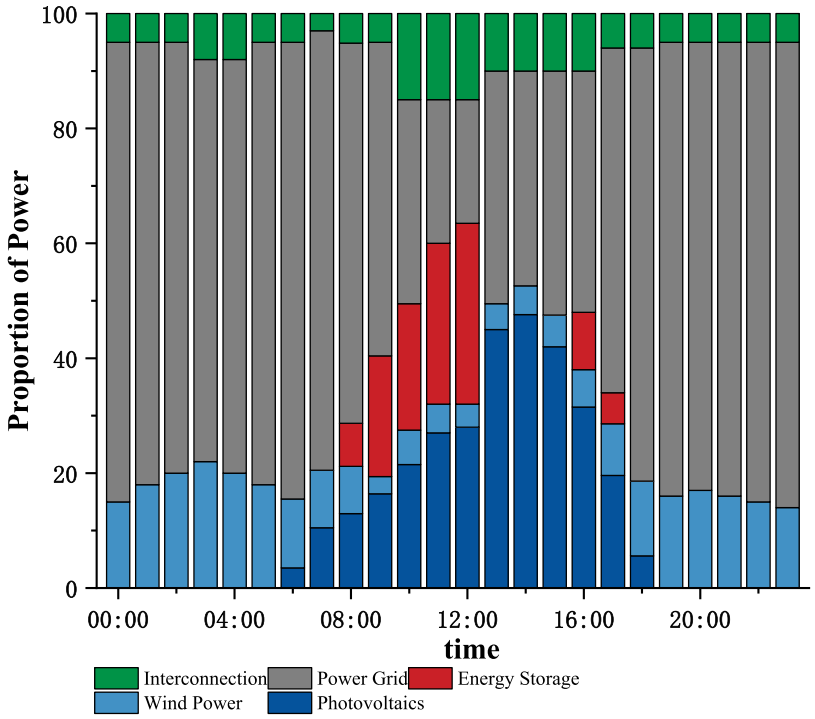


Figure 9: Generator output percentage diagram (After Optimization).

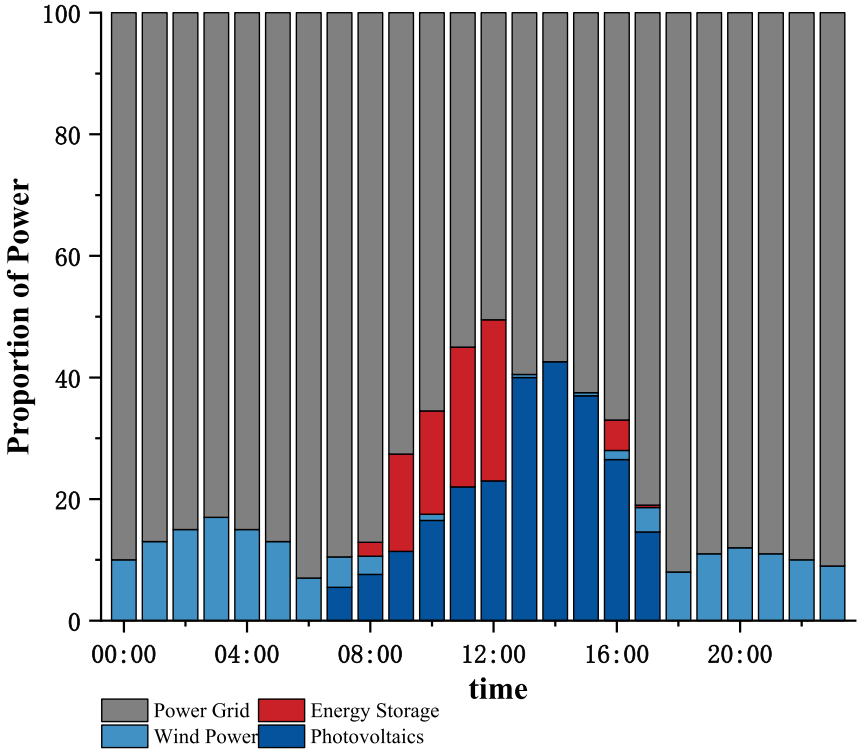


Figure 10: Generator output percentage diagram (Before Optimization).

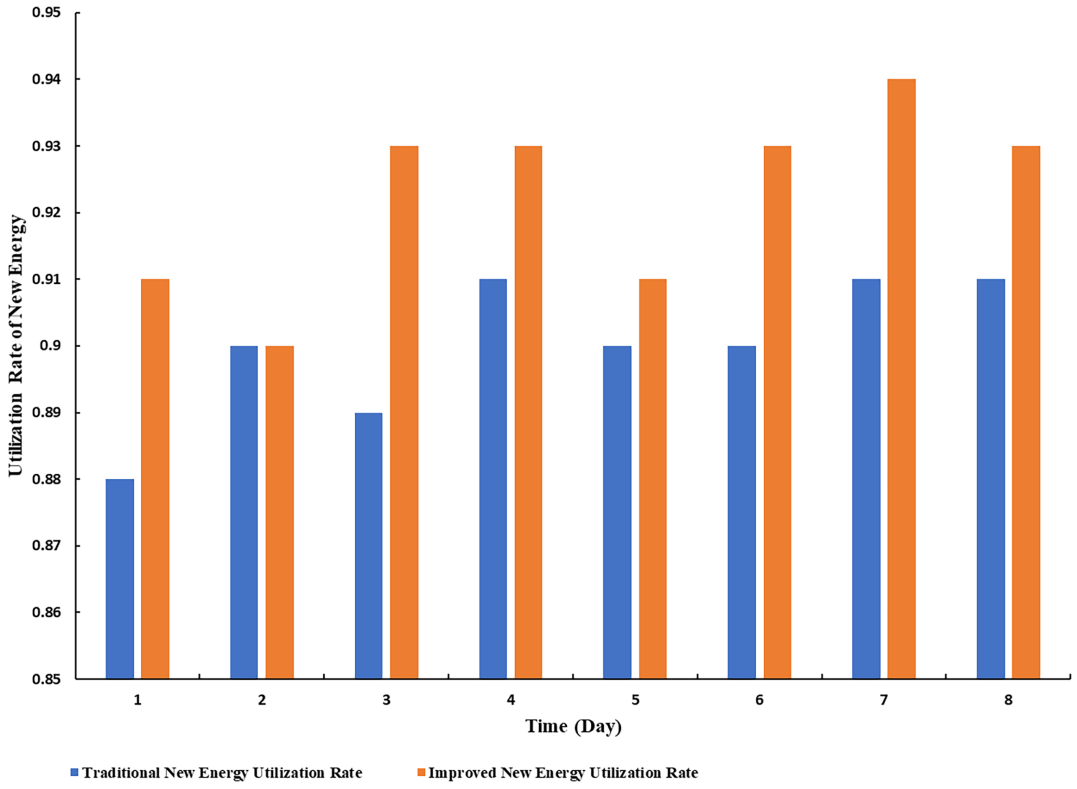


Figure 11: Renewable energy utilization rate diagram.

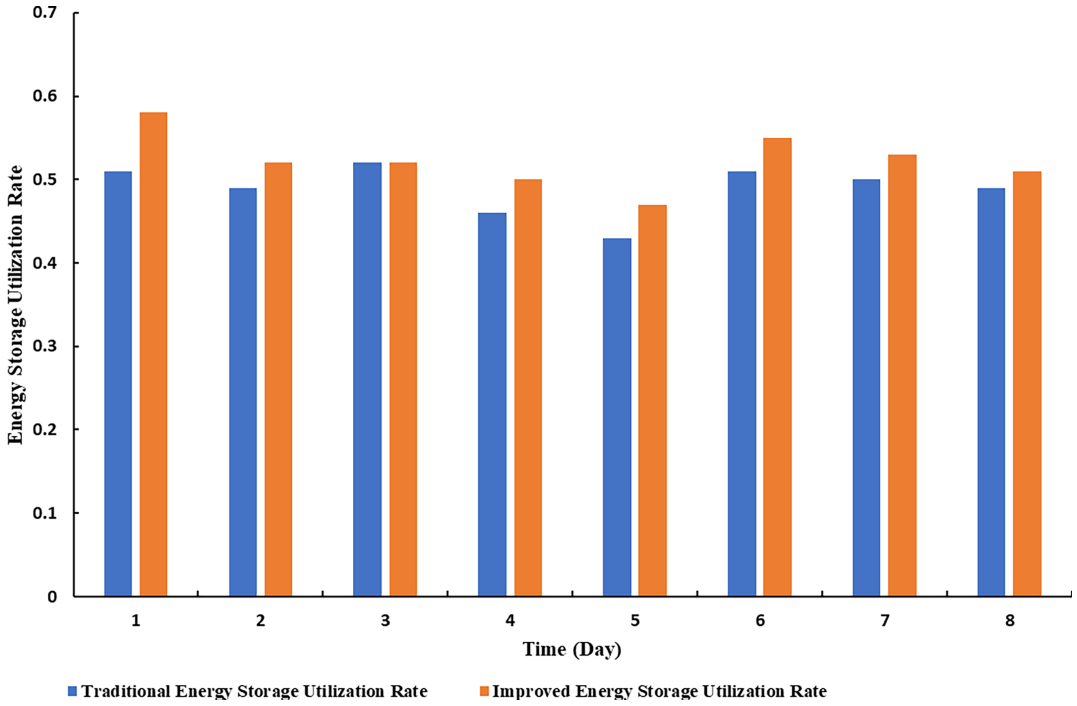


Figure 12: Energy storage utilization rate diagram.

The above figures illustrate the state of charge (SOC) changes and charge-discharge powers of the energy storage systems at each node, as shown in Figs. 13 and 14. Fig. 13 clearly demonstrates the coordinated dispatch effect of the energy storage systems under the dynamic partitioning mode: the SOC of the energy storage in each distribution transformer area is strictly controlled within the safe range of 0.1–0.9, presenting the law of "charging during off-peak periods, discharging during peak periods, and cross-district complementarity." To ensure optimal economy, during the late-night electricity price off-peak period, all energy storage systems in each area charge at a power of 0.3~0.1 MW, and the SOC gradually rises from the initial 0.5 to approximately 0.8, making full use of low-price electricity to store energy. During the morning peak hours (7:00–10:00), the energy storage systems in Areas 1 and 2 discharge to support local loads; meanwhile, the energy storage system in Area 2 transmits 0.2 MW of power to Area 3, and the SOC of the energy storage in each area synchronously drops to 0.1–0.3. During the midday period (12:00–14:00) when photovoltaic output is abundant, the discharge power of the energy storage systems decreases to 0 MW, and the distribution transformer areas are powered by renewable energy and the power grid. After photovoltaic power supply ceases in the evening (18:00–24:00), the energy storage systems first discharge and then charge until the end of the dispatch cycle. Fig. 15 illustrates the power variation of each node after interconnection. Through comparison, it can be observed that the system power becomes more balanced post-interconnection, which indirectly verifies that the method proposed in this paper can better utilize energy storage and promote renewable energy absorption.

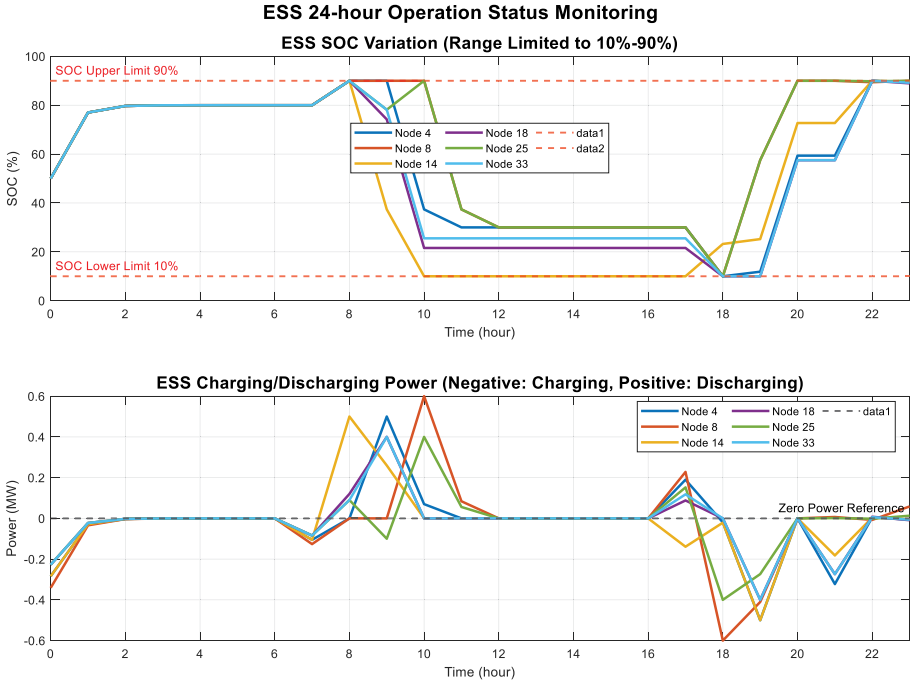


Figure 13: Energy storage parameter variation diagram.

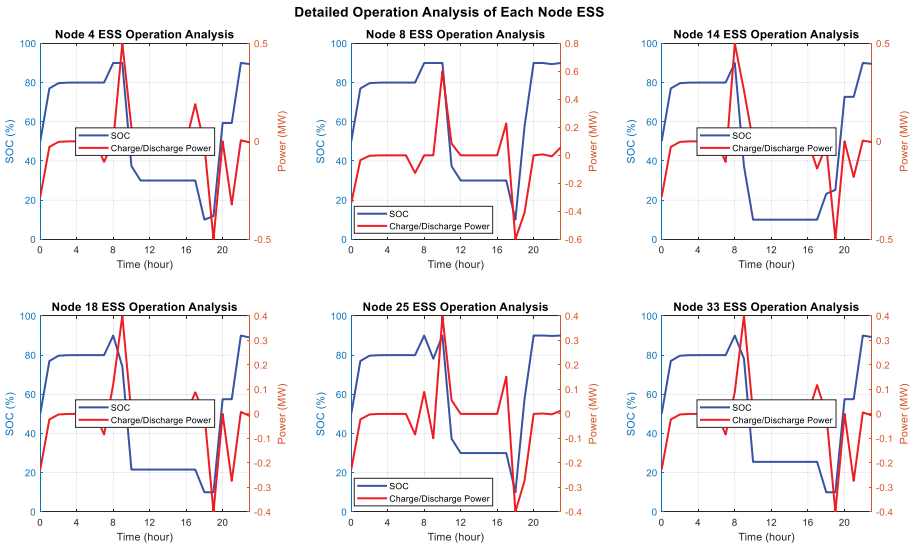


Figure 14: Energy storage parameter variation diagram.

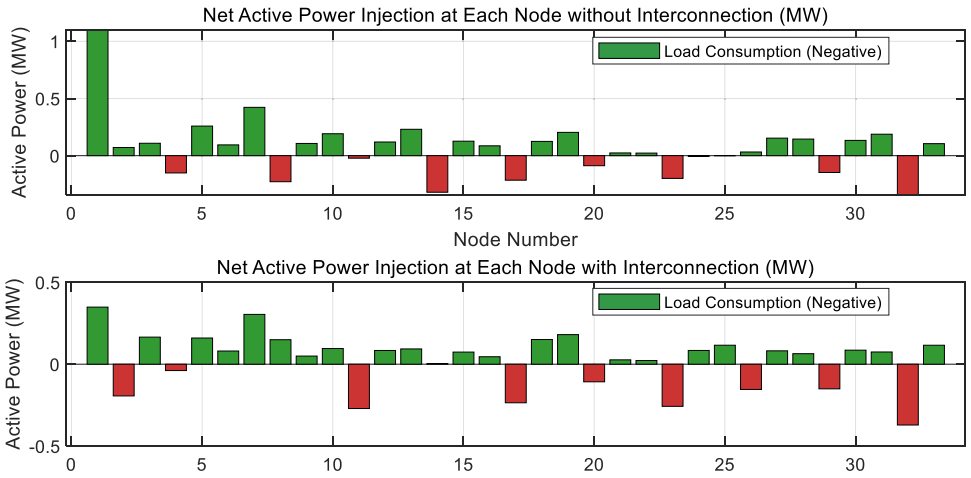


Figure 15: Power diagram of each node.

5 Conclusions

(1) Operational Economy: The dynamic optimal partitioning mode achieves relatively low operational costs. By optimizing power flow and energy storage dispatch, this mode better utilizes distributed renewable energy, reducing the power purchase demand from the external grid and internal system losses.

(2) Comprehensive Performance (Indicator Q): The comprehensive indicator Q integrates voltage stability and economic objectives. The dynamic optimal partitioning mode yields the lowest Q value, fully demonstrating its capability in synergistically optimizing multiple performance indicators and achieving the optimal overall system performance.

(3) Simulation results fully verify that the traditional static partitioning mode struggles to address the challenges posed by high-proportion renewable energy integration. In contrast, the interconnected district coordinated dispatch strategy based on regional dynamic partitioning proposed in this paper can adaptively

adjust the operational structure, realizing improvements in both renewable energy absorption and energy storage utilization efficiency.

Acknowledgement: Not applicable.

Funding Statement: The authors received no specific funding for this study.

Author Contributions: The authors confirm contribution to the paper as follows: Conceptualization, Ze'ang Ma and Jie Chen; methodology, Ze'ang Ma; validation, Ze'ang Ma; formal analysis, Ze'ang Ma; data curation, Ze'ang Ma; writing—original draft preparation, Ze'ang Ma; writing—review and editing, Jie Chen; visualization, Ze'ang Ma; supervision, Jie Chen; project administration, Shuai Lyu. All authors reviewed and approved the final version of the manuscript.

Availability of Data and Materials: The data that support the findings of this study are available from the Corresponding Author, Jie Chen, upon reasonable request.

Ethics Approval: Not applicable.

Conflicts of Interest: The authors declare no conflicts of interest.

References

1. Faraji J, Ketabi A, Hashemi-Dezaki H, Shafie-Khah M, Catalao JPS. Optimal day-ahead self-scheduling and operation of prosumer microgrids using hybrid machine learning-based weather and load forecasting. IEEE Access. 2020;8:157284–305. doi:10.1109/access.2020.3019562.
2. Park H, Lee SY. Optimal microgrid scheduling to provide operational flexibility in main grid operation. Energy Rep. 2020;6:172–6. doi:10.1016/j.egyr.2019.08.038.
3. Sefidgar-Dezfouli A, Joorabian M, Mashhour E. A multiple chance-constrained model for optimal scheduling of microgrids considering normal and emergency operation. Int J Electr Power Energy Syst. 2019;112:370–80. doi:10.1016/j.ijepes.2019.05.026.
4. Lu Q, Zeng HZ, Yin LF. Distributed multi-objective fast convergent heuristic algorithm for novel power systems dispatch. Appl Soft Comput. 2026;186(PD):114294. doi:10.1016/J.ASOC.2025.114294.
5. Pan LR, Yang X, Yuan SB, Li JA, Xue HW. Risk assessment of new distribution network dispatching operations considering multiple uncertain factors. Electronics. 2025;14(20):4012. doi:10.3390/ELECTRONICS14204012.
6. Ahshan R, Abid MS, Al Abri M. Multi-modal multi-task artificial intelligence model for active distribution network scheduling with multi-agent reinforcement learning. Electr Power Syst Res. 2026;250:112091. doi:10.1016/J.EPSR.2025.112091.
7. Wang YQ, Liu SF, Wang Y, Lv ZT, Liang J. Adaptive optimal dispatch of flexible interconnected distribution transformer areas based on operation state classification. Electr Power Autom Equip. 2024;44(12):10–7. (In Chinese). doi:10.16081/j.epae.202409023.
8. Liu KY, Sheng WX, Zhan HY. Bi-level coordinated optimal dispatch method for medium-low voltage AC/DC hybrid distribution networks considering multi-area interconnection. Electr Power Constr. 2024;45(1):33–44. (In Chinese).
9. Song X, Chen S, Zhao C, Zhang Z. Promoting open-source Calliope platform in planning and operation of shared energy storage-assisted microgrid clusters. Energy Convers Manag. 2026;348(4):120677. doi:10.1016/j.enconman.2025.120677.
10. Li X, Zhu L, Zhao L, Zhang K. Bi-objective operation optimization of regional integrated energy system considering shared energy storage. Sci Rep. 2025;15(1):38737. doi:10.1038/s41598-025-22502-4.
11. Hu H, Lu H, Zhao W, Cao X, Fan X, Jiang J. Optimization configuration method for shared energy storage considering economic consumption of new energy. Int J Electr Power Energy Syst. 2025;172(1):111117. doi:10.1016/j.ijepes.2025.111117.

12. Moretti L, Polimeni S, Meraldi L, Raboni P, Leva S, Manzolini G. Assessing the impact of a two-layer predictive dispatch algorithm on design and operation of off-grid hybrid microgrids. Renew Energy. 2019;143:1439–53. doi:10.1016/j.renene.2019.05.060.
13. Li M. Scenario analysis and key technologies of flexible interconnection for low-voltage distribution station areas. J Electr Technol. 2025;23:85–91. (In Chinese). doi:10.19768/j.cnki.dgjs.2025.23.023.
14. Liu X, Zhang W, Chi Z, Jiang T, Ji Y. Optimal energy scheduling for multi-energy network based on incentive integrated demand response. Sustain Energy Grids Netw. 2025;44(1):101986. doi:10.1016/j.segan.2025.101986.
15. Zhou SB, Xu ZY, Tang XQ. Method for determining optimal number of clusters in K-means algorithm. J Comput Appl. 2010;30(8):1995–8. doi:10.3724/sp.j.1087.2010.01995.
16. Gbadega PA, Sun Y, Balogun OA. Optimized energy management in Grid-Connected microgrids leveraging K-means clustering algorithm and Artificial Neural network models. Energy Convers Manag. 2025;336:119868. doi:10.1016/j.enconman.2025.119868.
17. Hussein HI, Ghadban AM, Muñoz FJ, Rodríguez A. Parallel computing for power quality disturbances analysis and energy management in distribution power networks. Arab J Sci Eng. 2025;49(5):7277. doi:10.1007/s13369-025-10224-8.
18. Kabe M, Bokovi Y, Sedzro KS, Takouda P, Lare Y. Optimal electrification using renewable energies: microgrid installation model with combined mixture k-means clustering algorithm, mixed integer linear programming, and onsset method. Energies. 2024;17(12):3022. doi:10.3390/en17123022.
19. Raj P, Richter E, Schofer K, Kempf J, Michel F, Fill A, et al. Lifetime prediction of Lithium-ion cells using electrochemical modeling with combined calendar and cyclic aging effects. E Prime Adv Electr Eng Electron Energy. 2025;14:101103. doi:10.1016/j.prime.2025.101103.
20. Wu SM, Guo H, Wang F, Zhang XK, Zhu YX. A hybrid data-model-driven framework for price-responsive energy storage dispatch in integrated energy systems. J Energy Storage. 2026;141(PA):119269. doi:10.1016/J.EST.2025.119269.
21. Zheng X, Ju C, Yang G, Chu J. Risk-aware collaborative optimization for quantity–price bidding and energy storage dispatch in virtual power plants. J Energy Storage. 2026;149:120112. doi:10.1016/j.est.2025.120112.
22. Hong L, Gao Y, Wu M, Xu C, Wu S, Du A. Optimization strategy for PV-hydrogen coordination in PV high-penetration distribution networks considering transformer lifetime consumption. Int J Hydrogen Energy. 2025;165:150688. doi:10.1016/j.ijhydene.2025.150688.
23. Diahovchenko I. Analyzing the influence of electric vehicle charging scheduling on distribution transformer lifespan. Heliyon. 2024;10(21):e39904. doi:10.1016/j.heliyon.2024.e39904.